

SPACECRAFT DYNAMICS ANALYSIS USING POINT-MASS MODEL OF HUMAN MOTION

Galen Bascom*, Leah Kiner†, and Hanspeter Schaub‡

As concepts for spacecraft with larger populations of humans aboard emerge, the need for an implementable model of the effects of human and cargo motion grows. A point-mass model for that motion is created, and the effects on spacecraft rotational and translational motion derived. Using a back-substitution method developed in previous work on multi-body dynamics, an efficient and modular software implementation of the dynamics is presented. The moving point mass along a spinning spacecraft hub is simulated, demonstrating complex attendant behaviors. The sensitivity of the effects on the hub to both the mass and speed of the moving object are investigated.

INTRODUCTION

The presence of humans and moving cargo aboard a spacecraft inevitably affects its motion, as the spacecraft hub experiences reactive forces and torques. These effects have long been recognized, with researchers since the 1960s working to investigate and quantify the effects of astronaut motion on spacecraft.^{1,2} In many cases, that early work focused on determining the stability of the ensuing multi-body systems. Other research has centered on experimental determination of the magnitudes of the forces and torques induced by human motion aboard the ISS and the *Mir* space station.^{2,3} These approaches provide useful insight that can be complemented by the development of an efficient and easily implemented software model for human motion in space.

New concepts for space missions are emerging that involve not only the actions of a few astronauts aboard a space station but also larger populations of humans living and working in space. For example, Blue Origin and Sierra Space have announced plans for a low-earth orbiting commercially owned space station.* Axiom Space plans to install new modules on the ISS as soon as 2025.† The motions of only a few humans aboard relatively large spacecraft result in correspondingly minor effects. However, those effects become more substantial when larger numbers of humans and heavy cargo are considered.

*PhD Student, Ann and H.J. Smead Department of Aerospace Engineering Sciences, University of Colorado, Boulder, Boulder, CO, 80309. AAS Member.

†PhD Student, Ann and H.J. Smead Department of Aerospace Engineering Sciences, University of Colorado, Boulder, Boulder, CO, 80309. AAS Member, AIAA Member.

‡Professor and Department Chair, Schaden Leadership Chair, Ann and H.J. Smead Department of Aerospace Engineering Sciences, University of Colorado, Boulder, 431 UCB, Colorado Center for Astrodynamics Research, Boulder, CO, 80309. AAS Fellow, AIAA Fellow.

*<https://www.blueorigin.com/news/orbital-reef-commercial-space-station/>

†<https://spacenews.com/commercial-space-station-developers-seek-clarity-on-regulations/>



Figure 1. Artist's concept image of Axiom Station.*

This work revisits the problem of moving masses aboard spacecraft, first developing a dynamic model of the motion. It implements software modules for modeling those effects within an architecture designed to achieve modularity and computational efficiency. This allows the investigation of the effects of moving masses on large space stations. In particular, it helps to determine what magnitude of disturbances are caused by such motion, such as wobbles in the spin axis or shifts of the space station center of mass. Expanding the capability to simulate human activity and other complex multi-body dynamics will enable future work to evaluate stability, quantify disturbances, and design concepts for humans and other moving masses aboard large habitats in space.

DYNAMICS

The analytical approach taken here begins with the full derivation of the equations of motion for the coupled multi-body system. The linear and angular momentum of the system as a whole are conserved in the absence of external forces, but moving masses cause forces and torques on the rigid space station. Researchers have developed sophisticated models of the dynamics of a human body in space, including complex changes to the body's moment of inertia.^{4,5} Adding additional degrees of freedom greatly increases complexity both for deriving the equations of motion and for specifying the motions in particular simulations. Here, the model chosen for the moving mass is a point mass with negligible inertia. This serves as a useful first approximation for both human and cargo motion aboard the space station that is orders of magnitude larger.

The basic problem setup consists of a system of two masses, one rigid spacecraft hub and one mass whose motion is prescribed relative to the hub using reaction forces against the hub. The schematic for the two masses is shown in Figure 2. This latter is designated the moving mass, although of course both masses move. The rotational and translational motion of the hub are affected by the moving mass's prescribed motion, that is the specified position, velocity and acceleration of the mass with respect to the hub. A full derivation of the six-degree-of-freedom dynamics for

*<https://www.axiomspace.com/news-and-media>

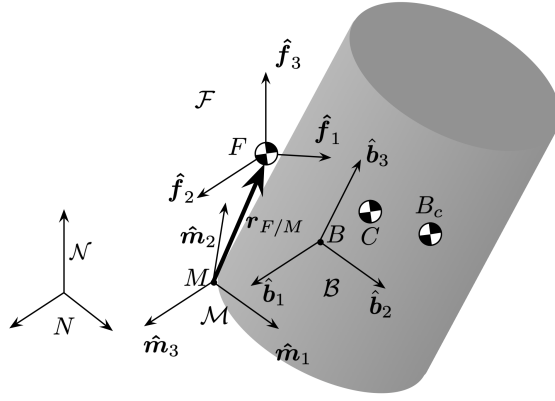


Figure 2. Geometry and coordinate frames.

prescribed motion and the attendant software implementation are given in a forthcoming paper,⁶ with relevant steps described here.

Frame Definitions

The inertial frame is defined $\mathcal{N} : \{N, \hat{n}_1, \hat{n}_2, \hat{n}_3\}$, as well as a hub-fixed frame $\mathcal{B} : \{B, \hat{b}_1, \hat{b}_2, \hat{b}_3\}$. The point B can be any body-fixed point, with B_c the known hub center of mass. The moving-mass fixed frame is $\mathcal{F} : \{F, \hat{f}_1, \hat{f}_2, \hat{f}_3\}$, with F_c the known center of mass. In this study F coincides with F_c , as the human or cargo is assumed to be a point mass. For the same reason, the frame \mathcal{F} is not a consideration because the orientation is held fixed in this study. But for the full dynamics derivation, this frame is necessary to describe relative orientation. Finally, the particle motion is described relative to a second body-fixed frame $\mathcal{M} : \{M, \hat{m}_1, \hat{m}_2, \hat{m}_3\}$. This is done for convenience, as the primary body frame \mathcal{B} is not always the most convenient reference frame in which to express the particle motion.

The prescribed parameters are $\mathbf{r}_{F/M}$, the position of the mass relative to the intermediate frame, $\mathbf{r}'_{F/M}$, the body-frame velocity of the mass, and $\mathbf{r}''_{F/M}$ its body-frame acceleration. Prime notation refers to body frame derivatives, with dot notation representing inertial derivatives. Because the \mathcal{B} and \mathcal{M} frames are fixed relative to each other, with both are fixed to the body,

$$\frac{\mathcal{B}d(\cdot)}{dt} = (\cdot)' = \frac{\mathcal{M}d(\cdot)}{dt} \quad (1)$$

Note that the full derivation also includes prescribed attitude, rate of rotation, and rotational acceleration of the moving mass; those quantities are omitted here, as we assume negligible inertia.

Translational Motion

The derivation of the translational dynamics begins with Newton's second law:⁷

$$m_{sc}\ddot{\mathbf{r}}_{C/N} = m_{sc}(\ddot{\mathbf{r}}_{B/N} + \ddot{\mathbf{c}})\mathbf{F}_{ext} \quad (2)$$

The notation $\mathbf{r}_{C/N}$ denotes the location of point C with respect to N , and \mathbf{F}_{ext} the sum of the external forces. The vector \mathbf{c} is defined as the overall system center of mass:

$$\mathbf{c} = \mathbf{r}_{C/B} = \frac{m_{\text{hub}}\mathbf{r}_{B_c/B} + m_{\text{P}}\mathbf{r}_{F_c/B}}{m_{\text{sc}}} \quad (3)$$

Note that

$$\mathbf{r}_{F_c/B} = \mathbf{r}_{F/B} = \mathbf{r}_{F/M} + \mathbf{r}_{M/B} \quad (4)$$

and, as a consequence:

$$\mathbf{r}'_{F/B} = \mathbf{r}'_{F/M} + \mathbf{r}'_{M/B} = \mathbf{r}'_{F/M} \quad (5)$$

This in turn gives us the simplified form of the body-frame derivative of \mathbf{c} :

$$\mathbf{c}' = \frac{m_{\text{P}}\mathbf{r}'_{F/M}}{m_{\text{sc}}} \quad (6)$$

After intermediate steps and simplification to express $\ddot{\mathbf{r}}_{C/N}$ in terms of known quantities, it can be shown⁶ that the translational equations of motion can be written as:

$$m_{\text{sc}}\ddot{\mathbf{r}}_{B/N} + m_{\text{sc}}[\dot{\tilde{\omega}}_{\mathcal{B}/\mathcal{N}}]\mathbf{c} = \mathbf{F}_{\text{ext}} - m_{\text{P}}\mathbf{r}''_{F_c/B} - 2m_{\text{sc}}[\tilde{\omega}_{\mathcal{B}/\mathcal{N}}]\mathbf{c}' - m_{\text{sc}}[\tilde{\omega}_{\mathcal{B}/\mathcal{N}}]^2\mathbf{c} \quad (7)$$

The notation $[\tilde{\omega}_{\mathcal{B}/\mathcal{N}}]$ represents a cross-product equivalent matrix for the rotational rate of frame \mathcal{B} with respect to frame \mathcal{N} . For the point mass a further simplification is possible:

$$\mathbf{r}''_{F_c/B} = \left([\tilde{\omega}'_{\mathcal{F}/\mathcal{B}}] + [\tilde{\omega}_{\mathcal{F}/\mathcal{B}}]^2\right)\mathbf{r}_{F_c/F} + \mathbf{r}''_{F/M} = \mathbf{r}''_{F/M} \quad (8)$$

yielding the equation:

$$m_{\text{sc}}\ddot{\mathbf{r}}_{B/N} + m_{\text{sc}}[\dot{\tilde{\omega}}_{\mathcal{B}/\mathcal{N}}]\mathbf{c} = \mathbf{F}_{\text{ext}} - m_{\text{P}}\mathbf{r}''_{F/M} - 2m_{\text{sc}}[\tilde{\omega}_{\mathcal{B}/\mathcal{N}}]\mathbf{c}' - m_{\text{sc}}[\tilde{\omega}_{\mathcal{B}/\mathcal{N}}]^2\mathbf{c} \quad (9)$$

Rotational Motion

The rotational equations of motion are derived in similar fashion, starting from first principles:⁷

$$\dot{\mathbf{H}}_{\text{sc},B} = \mathbf{L}_B + m_{\text{sc}}(\ddot{\mathbf{r}}_{B/N} \times \mathbf{c}) \quad (10)$$

where $\mathbf{H}_{\text{sc},B}$ is the angular momentum about B and \mathbf{L}_B is the net torque about B .

The angular momentum vector about point B can be shown⁶ (with some substitutions and simplifications) to take the form:

$$\mathbf{H}_{\text{sc},B} = [I_{\text{sc},B}]\boldsymbol{\omega}_{\mathcal{B}/\mathcal{N}} + [I_{\text{P},F_c}]\boldsymbol{\omega}_{\mathcal{F}/\mathcal{B}} + m_{\text{P}}[\tilde{\mathbf{r}}_{F_c/B}]\mathbf{r}'_{F_c/B} \quad (11)$$

Inertia quantities are denoted $[I_{\text{sc},B}]$ for the moment of inertia of the full system about point B , for example. Body frame derivatives of inertia quantities denoted the same way as for vector quantities with $'$ symbols. For the point mass, this equation simplifies:

$$\mathbf{H}_{\text{sc},B} = [I_{\text{sc},B}]\boldsymbol{\omega}_{\mathcal{B}/\mathcal{N}} + m_{\text{P}}[\tilde{\mathbf{r}}_{F_c/B}]\mathbf{r}'_{F/M} \quad (12)$$

After additional intermediate steps to differentiate the angular momentum vector and express all terms as known quantities, the rotational equations of motion are found:⁶

$$m_{sc}[\tilde{\mathbf{c}}]\ddot{\mathbf{r}}_{B/N} + [I_{sc,B}]\dot{\boldsymbol{\omega}}_{B/N} = \mathbf{L}_B - m_P[\tilde{\mathbf{r}}_{F_c/B}]\mathbf{r}_{F_c/B}'' - \left([I'_{sc,B}] + [\tilde{\boldsymbol{\omega}}_{B/N}][I_{sc,B}]\right)\boldsymbol{\omega}_{B/N} - \left([I'_{P,F_c}] + [\tilde{\boldsymbol{\omega}}_{B/N}][I_{P,F_c}]\right)\boldsymbol{\omega}_{F/B} - [I_{P,F_c}]\boldsymbol{\omega}'_{F/B} - m_P[\tilde{\boldsymbol{\omega}}_{B/N}][\tilde{\mathbf{r}}_{F_c/B}]\mathbf{r}'_{F_c/B} \quad (13)$$

For the point mass, further simplifications can be made:

$$m_{sc}[\tilde{\mathbf{c}}]\ddot{\mathbf{r}}_{B/N} + [I_{sc,B}]\dot{\boldsymbol{\omega}}_{B/N} = \mathbf{L}_B - m_P[\tilde{\mathbf{r}}_{F_c/B}]\mathbf{r}_{F/M}'' - \left([I'_{sc,B}] + [\tilde{\boldsymbol{\omega}}_{B/N}][I_{sc,B}]\right)\boldsymbol{\omega}_{B/N} - m_P[\tilde{\boldsymbol{\omega}}_{B/N}][\tilde{\mathbf{r}}_{F_c/B}]\mathbf{r}'_{F/M} \quad (14)$$

SOFTWARE IMPLEMENTATION

Prior work by Allard and Schaub in multi-body spacecraft dynamics uses a back-substitution method to retain the fully coupled dynamics of spacecraft with moving parts while achieving computational efficiency.^{8,9} The back-substitution method involves computing the contributions to the hub equations of motion by the other body in the coupled system, solving that reduced form of the problem, and then substituting the results back into the equations for the other body. This work employs that same technique. The equations of motion for the point mass coupled with a rigid spacecraft hub, Equations 9 and 13, are implemented in Basilisk,* a software architecture that uses back-substitution to be both modular and efficient.

The moving mass dynamics are implemented in a state effector Basilisk dynamics module, which communicates with the spacecraft as the states are integrated in time. The prescribed point mass kinematics are read in as an input message at each module time step, and the acceleration is held constant over the integration period. In order to prescribe the motion, separate flight software profiler modules were written to define the position, velocity, and acceleration of the moving particle at each moment in time.

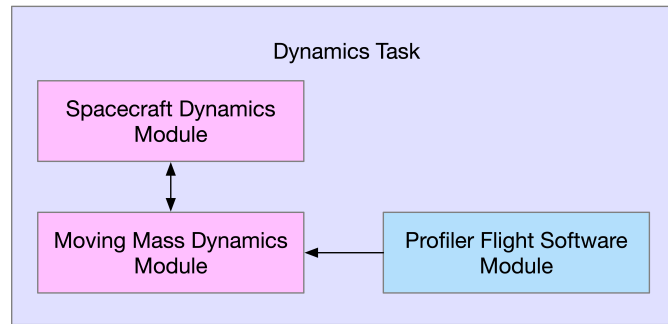


Figure 3. Basilisk module interconnections for simulation setup.

Linear Motion Profiler

The linear motion profiler takes as parameters the starting and ending positions of the moving mass, as well as a maximum acceleration a_{max} and a maximum speed v_{max} . It calculates the

*<https://hanspeterschaub.info/basilisk>

direction of motion:

$$\Delta \mathbf{r} = \mathbf{r}_{F/M}(t_f) - \mathbf{r}_{F/M}(t_s) \quad (15)$$

With a user-specified starting time t_s , the logic of the module determines the amount of time spent in an acceleration phase t_{accel} to reach v_{max} and the amount of time spent in a coast phase. The time to decelerate is also t_{accel} .

Define t_s as the starting time, t_1 as the time when acceleration turns off, t_2 as the time when deceleration begins, and t_f as the time when the motion is complete. During the acceleration phase,

$$\mathbf{r}_{F/M}(t) = \mathbf{r}_{F/M}(t_s) + \frac{1}{2}a_m(t - t_s)^2\Delta \mathbf{r} \quad (16)$$

$$\mathbf{r}'_{F/M}(t) = a_m(t - t_s)\Delta \mathbf{r} \quad (17)$$

$$\mathbf{r}''_{F/M}(t) = a_m\Delta \mathbf{r} \quad (18)$$

The position increases quadratically, and the direction is in a straight line between the starting and ending positions.

During the coast phase, the velocity is constant while the position increases linearly:

$$\mathbf{r}_{F/M}(t) = \mathbf{r}_{F/M}(t_1) + v_m(t - t_1)\Delta \mathbf{r} \quad (19)$$

$$\mathbf{r}'_{F/M}(t) = v_m(t - t_1)\Delta \mathbf{r} \quad (20)$$

$$\mathbf{r}''_{F/M}(t) = 0 \quad (21)$$

This phase does not affect the motion of the hub, as there is no acceleration by the moving mass.

During deceleration, the acceleration is negative, velocity decreases linearly, and the position increases as concave downward quadratic:

$$\mathbf{r}_{F/M}(t) = \mathbf{r}_{F/M}(t_2) + \left(v_m(t - t_2) - \frac{1}{2}a(t - t_2)^2 \right) \Delta \mathbf{r} \quad (22)$$

$$\mathbf{r}'_{F/M}(t) = (v_m - a(t - t_2)) \Delta \mathbf{r} \quad (23)$$

$$\mathbf{r}''_{F/M}(t) = -a\Delta \mathbf{r} \quad (24)$$

Circular Motion Profiler

The circular motion profiler assumes the particle is undergoing a circular motion relative to a body-fixed point. It takes as parameters the starting position of the moving mass and the overall circular distance to be traveled, with the direction assumed to be circular and about the $\hat{\mathbf{f}}_3$ axis in the \mathcal{F} frame (which stays aligned with the \mathcal{B} frame for the point mass case). Like the linear profiler, it also has a configurable maximum tangential acceleration and maximum speed. The tangential motion follows essentially the same profile as in the linear case. However, the position and velocity directions are calculated based on the overall angular displacement over time. Scalar linear terms for the position, velocity and acceleration are calculated. During acceleration, these are:

$$r(t) = r_s + \frac{1}{2}a_m(t - t_s)^2 \quad (25)$$

$$v(t) = a_m(t - t_s) \quad (26)$$

$$a(t) = a_m \quad (27)$$

During coast, they become:

$$r(t) = r_1 + v_m(t - t_1) \quad (28)$$

$$v(t) = v_m \quad (29)$$

$$a(t) = 0 \quad (30)$$

And during deceleration:

$$r(t) = r_2 + v_m(t - t_s) - \frac{1}{2}a_m(t - t_2)^2 \quad (31)$$

$$v(t) = v_m - a_m(t - t_2) \quad (32)$$

$$a(t) = -a_m \quad (33)$$

These scalar quantities are then used to calculate the overall vector quantities:

$$\Delta\theta(t) = \frac{r(t)}{R} \quad (34)$$

$$\mathbf{r}_{F/M}(t) = \begin{bmatrix} \cos(\theta_s + \Delta\theta(t)) \\ \sin(\theta_s + \Delta\theta(t)) \\ z_s \end{bmatrix} \quad (35)$$

$$\mathbf{r}'_{F/M}(t) = v(t) \cdot \begin{bmatrix} -\sin(\theta_s + \Delta\theta(t)) \\ \cos(\theta_s + \Delta\theta(t)) \\ 0 \end{bmatrix} \quad (36)$$

$$\mathbf{r}''_{F/M}(t) = \mathbf{a}_c(t) + a(t) \cdot \begin{bmatrix} -\sin(\theta_s + \Delta\theta(t)) \\ \cos(\theta_s + \Delta\theta(t)) \\ 0 \end{bmatrix} \quad (37)$$

The centripetal acceleration is calculated using the radius of motion R as:

$$\mathbf{a}_c(t) = -\frac{v(t)^2}{R} \frac{\mathbf{r}_{F/M}(t)}{\|\mathbf{r}_{F/M}(t)\|} \quad (38)$$

RESULTS

Simulation Setup

The simulation is of a large cylindrical space station in deep space, not affected by any other gravitational bodies or perturbations. Its initial state is freely spinning in a stable manner about a principal axis, and it is not otherwise controlled. The moment of inertia and mass of the station hub are set by assuming a cylinder diameter of 25 m, a height of 50 m, and calculating a rough mass and density that would correspond to a large metal structure of those dimensions. The intent is to demonstrate order of magnitude effects of translational and rotational perturbations and provide a basis of comparison. The final space station mass is taken to be 2.0×10^6 kg, with an inertia of:

$$I_{\text{hub}} = \begin{bmatrix} 5.0 \times 10^8 & 0.0 & 0.0 \\ 0.0 & 5.0 \times 10^8 & 0.0 \\ 0.0 & 0.0 & 1.6 \times 10^8 \end{bmatrix} \text{ kg} \cdot \text{m}^2 \quad (39)$$

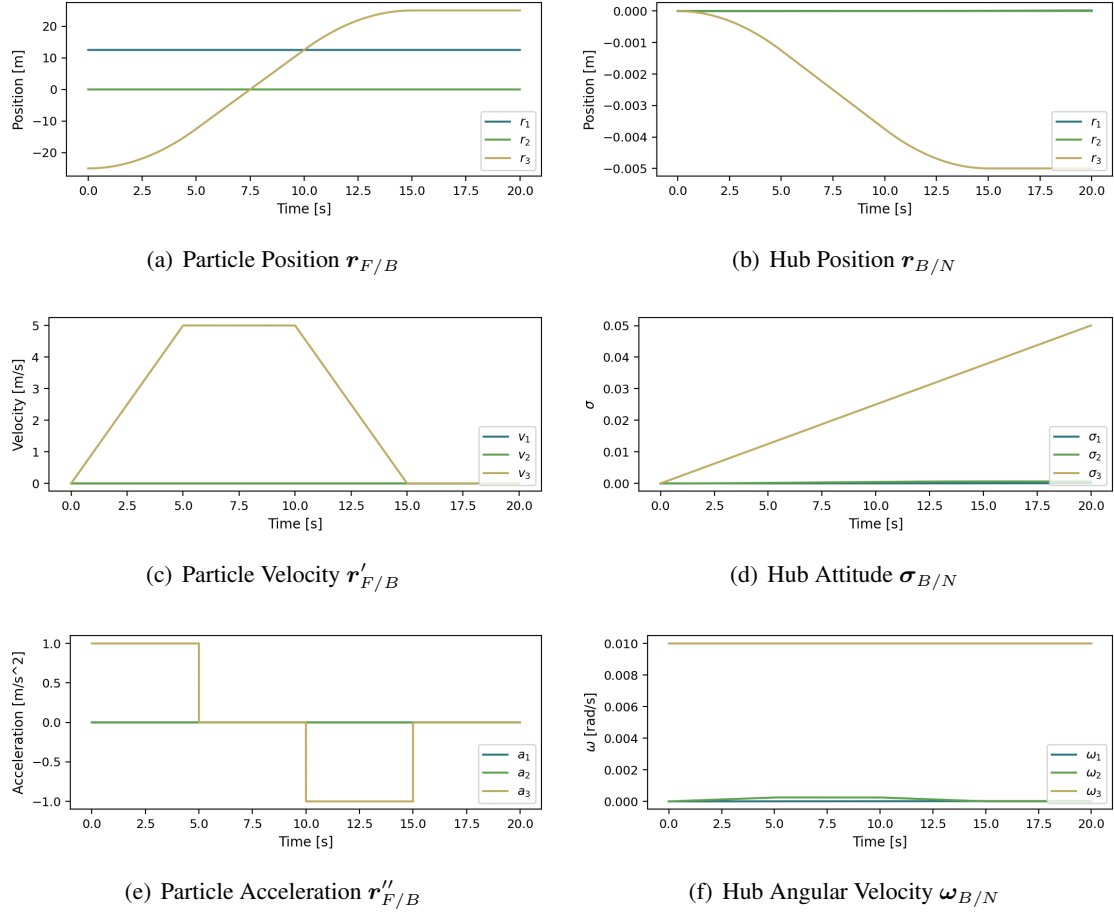


Figure 4. Kinematic states of moving mass and space station hub for the linear motion case.

The spacecraft hub's initial angular rate is taken to be 0.01 radians per second (about 0.57 degrees per second) about the \hat{b}_3 axis.

The moving mass is assumed to be some object, such as humans or cargo, moving along a linear or circular track inside an elevator or similar structure. The particle mass varies between 200 to 2000 kg. Its maximum acceleration is 1.0 m/s^2 , and its maximum speed varies between 0.5 and 5.0 m/s. The \mathcal{M} frame is taken to be identical to the \mathcal{B} frame.

Simulation Results for Fixed Parameters

The overall effects on the spacecraft are examined for two scenarios (1) moving from the top to the bottom along the \hat{b}_3 -axis (from -25.0 m to 25.0 m with the \mathcal{B} frame origin at the cylinder center of mass) and (2) walking in a circular path around the circumference at a height of 0 m . In all cases, the starting \hat{b}_1 position is 12.5 m and the starting \hat{b}_2 position is 0.0 m . The chosen variable parameters for the initial simulation result use a mass of 2000 kg and a maximum speed of 5.0 m/s .

For the case of linear motion from the top to the bottom of the cylinder, shown in Figure 4, the profiles are of the constant-acceleration body-frame motion described by the linear profiler. The \hat{b}_1 and \hat{b}_2 positions do not change, while the \hat{b}_3 position varies from -25.0 m to 25.0 m by parabolic arcs

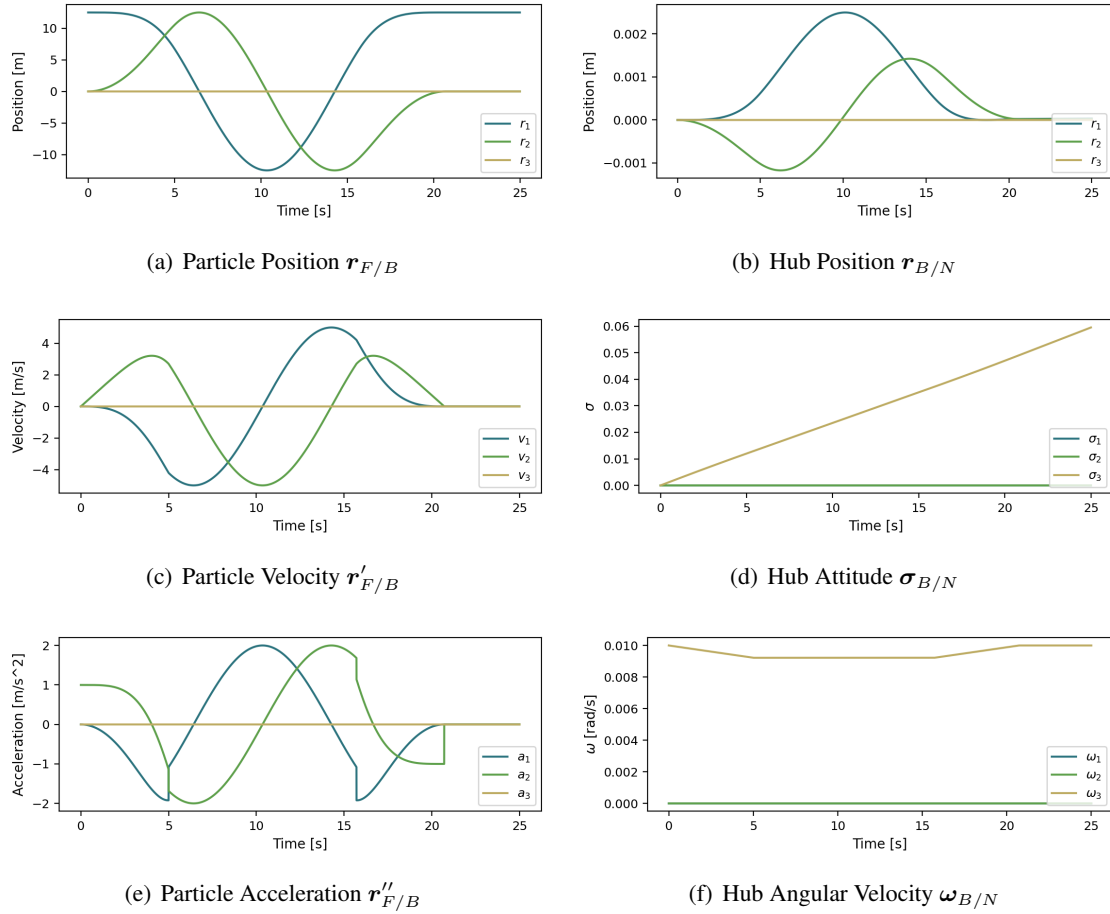


Figure 5. Kinematic states of moving mass and space station hub for the circular motion case.

connected by a linear portion. The velocity is linearly increasing and decreasing during periods of nonzero constant acceleration. As for the effects on the hub, small changes in the linear position on the order of 5.0×10^{-3} m are seen. Without the moving mass, the positions would stay at 0.0 for all time. The attitude, shown as modified Rodrigues parameters (MRPs), would have zero change in σ_2 and σ_3 , and a linear increase in σ_1 until the MRP switch happened after half a revolution. Similarly, the angular rates would stay constant, but instead slight variations in the direction can be seen during the motion.

For the case of circular motion about the circumference of the cylinder, the body-frame motion is somewhat more complex. For uniform circular motion, the position and velocity would be perfect sine and cosine functions; instead, the effects of the tangential acceleration are also seen. While the tangential acceleration has a maximum magnitude, 1.0 m/s^2 , there is no maximum magnitude to the centripetal acceleration needed to keep the motion circular, and indeed the magnitude of the acceleration is high during the coast period due to the high body-frame velocity. The acceleration and deceleration periods are marked by the discontinuities in the acceleration profile. The position of the hub is also affected in the \hat{n}_1 and \hat{n}_2 components by the motion around the circle (note that originally, the \mathcal{N} frame is aligned with the \mathcal{B} frame). Also, during the counterclockwise motion of the moving mass, the positive \hat{b}_3 -axis spin is noticeably reduced.

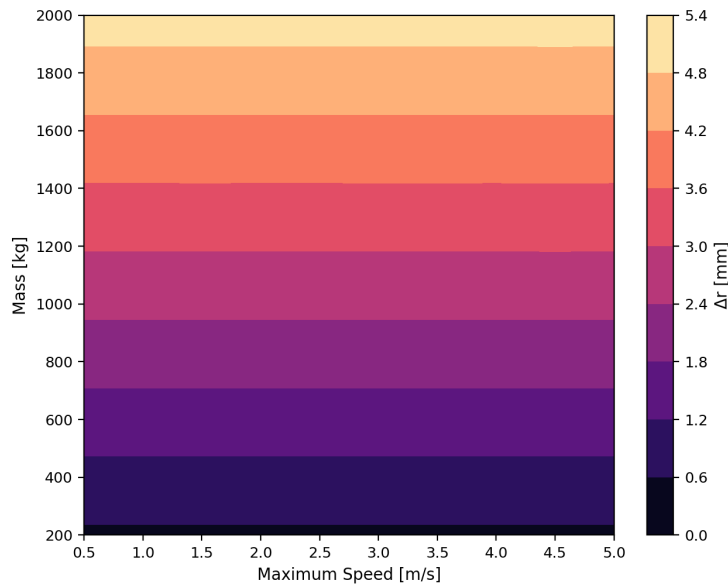


Figure 6. Norm of the hub position change as mass and maximum speed vary for linear motion.

Varying Mass and Speed Parameters

To look at the sensitivity of the effects on the hub to some of the moving mass parameters, the mass was varied from 200 to 2000 kg and the maximum speed from 0.5 to 5.0 m/s. It would also be of interest to investigate changing the shape and dimensions of the spacecraft hub, as well as more complex motions and paths. For these purposes, however, varying the mass and maximum speed give some indication of the relative magnitude of the effects. For the linear motion described, the simulation was run for 120 seconds, allowing the motion to fully complete for all cases, and the overall hub position evaluated. For both the linear and circular motion, the change in the angular acceleration was evaluated at its peak, just after the completion of the acceleration of the moving mass.

For the change in the overall position due to linear motion, shown in Figure 6, the maximum speed has no effect. This is because, if the mass and distance traveled are held fixed, and knowing that the overall system center of mass does not change, the hub position must always change the same amount to compensate for the moving mass. Of course, the maximum speed changes how quickly this translational motion happens. As expected, increased mass has a bigger effect, up to the order of 5 mm.

When it comes to the change in the magnitude of the angular acceleration from the linear path along the \hat{b}_3 axis, shown in Figure 7, the maximum speed is now as relevant as the mass. For the maximum speed and mass chosen, the effect on the norm was on the order of 0.01 degrees per second. This is substantial, in particular noting the original angular velocity norm is 0.57 degrees per second.

Finally, for the change in the magnitude of the angular acceleration when the mass was moving about the circumference, shown in Figure 8, the maximum effects were even larger. The direction chosen was always the same, so these effects went to decrease the spin magnitude. Of course, if the

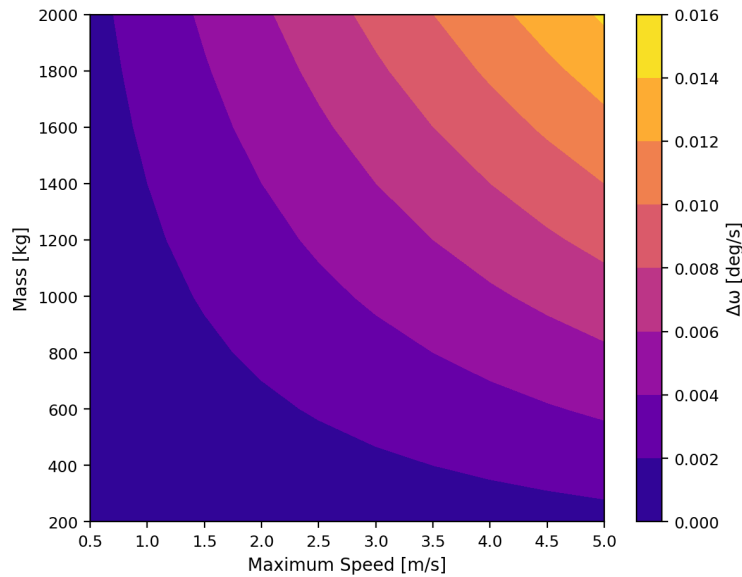


Figure 7. Norm of the change to the hub angular velocity as mass and maximum speed vary for linear motion.

mass were moving in the other direction, the angular acceleration would be expected to increase.

CONCLUSION

A model of human and cargo motion aboard spacecraft was developed, and the full dynamics derived. Those dynamics were implemented in software and a spacecraft hub with a moving mass following prescribed motion simulated. For both linear and circular motion and for the parameters chosen, nontrivial effects on the hub position and angular velocity were demonstrated. Future work involves varying additional parameters of the simulation, looking at the effects while the spacecraft is in orbit, and investigating more complex spacecraft geometries and moving mass trajectories.

REFERENCES

- [1] A. R. Amir and D. J. Newman, "Research Into the Effects of Astronaut Motion on the Spacecraft: A Review," *Acta Astronautica*, Vol. 47, No. 12, 2000, pp. 859–869.
- [2] D. J. Newman, A. R. Amir, and S. M. Beck, "Astronaut-Induced Disturbances to the Microgravity Environment of the *Mir* Space Station," *Journal of Spacecraft and Rockets*, Vol. 38, No. 4, 2001, pp. 578–583.
- [3] A. R. Amir, G. Baroni, A. Pedrocchi, D. J. Newman, G. Ferrigno, and A. Pedotti, "Measuring Astronaut Performance on the ISS: Advanced Kinematic and Kinetic Instrumentation," *IEEE Transactions on Instrumentation and Measurement*, Vol. 50, No. 5, 2001, pp. 1450–1455.
- [4] H. Li, Y. Jin, and C. Wang, "Modeling and Simulation of Astronaut Motions during Extravehicular Activity: A Complex System Based Method," *AASRI Procedia*, Vol. 3, 2012, pp. 118–126.
- [5] L. Stirling, K. Willcox, and D. Newman, "Development of a computational model for astronaut reorientation," *Journal of Biomechanics*, Vol. 43, 2010, pp. 2309–2314.
- [6] L. Kiner, J. V. Carneiro, C. Allard, and H. Schaub, "Spacecraft Simulation Software Implementation of General Prescribed Motion Dynamics of Two Connected Rigid Bodies," AAS Rocky Mountain GN&C Conference, Breckenridge, CO, Feb. 2–8, 2023, forthcoming.
- [7] H. Schaub and J. L. Junkins, *Analytical Mechanics of Space Systems*. Reston, Virginia: American Institute of Aeronautics and Astronautics, Inc., 4 ed., 2018.

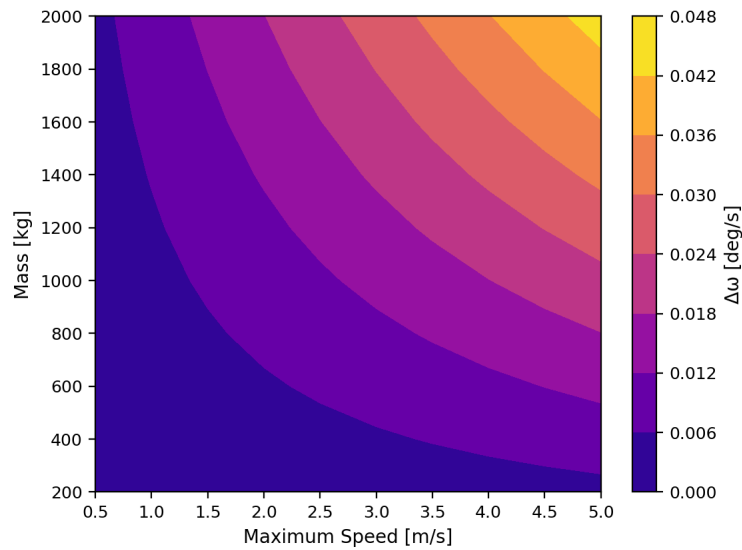


Figure 8. Norm of the change to the hub angular velocity as mass and maximum speed vary for circular motion about the hub circumference.

- [8] C. Allard, M. D. Ramos, H. Schaub, P. Kenneally, and S. Piggott, “Modular Software Architecture for Fully Coupled Spacecraft Simulations,” *Journal of Aerospace Information Systems*, Vol. 15, No. 12, 2018, pp. 670–683.
- [9] C. Allard, H. Schaub, and S. Piggott, “General Hinged Rigid-Body Dynamics Approximating First-Order Spacecraft Solar Panel Flexing,” *Journal of Spacecraft and Rockets*, Vol. 55, No. 5, 2018, pp. 1290–1298.